Oxidized Derivatives of *Octopus vulgaris* and *Carcinus aestuarii* Hemocyanins at pH 7.5 and Related Models by X-ray Absorption Spectroscopy

Elena Borghi,* Pier Lorenzo Solari,*† Mariano Beltramini,‡§ Luigi Bubacco,§ Paolo Di Muro,§ and Benedetto Salvato‡§

*Dipartimento di Chimica, Università "La Sapienza," I-00185 Roma, Italy; †General Purpose Italian Beam Line for X-ray Diffraction and Absorption Collaborating Research Group, European Synchrotron Radiation Facility, F-38043 Grenoble, France; ‡Dipartimento di Biologia, and ¶Consiglio Nazionale delle Ricerche, Center for Metalloproteins, Università di Padova, I-35121 Padova, Italy

ABSTRACT The binuclear copper sites of the met and met-azido derivatives of *Octopus vulgaris* and *Carcinus aestuarii* hemocyanins at pH 7.5 were characterized by high-resolution x-ray absorption spectroscopy in the low energy region (XANES) and in the higher region (EXAFS). The accuracy of the analysis of the data was tested with two mononuclear and six binuclear copper(II) complexes of the poly(benzimidazole) ligand systems 2-BB, L-5,5 and L-6,6 (Casella et al., 1993, *Inorg. Chem.* 32:2056–2067; 1996, *Inorg. Chem.* 35:1101–1113). Their structural and reactivity properties are related to those of the protein's derivatives. The results obtained for those models with resolved x-ray structure (the 2-BB-aquo and azido mononuclear complexes, and the binuclear L-5,5 Cu(II)-bis(hydroxo) (Casella et al., unpublished)), extends the validity of our approach to the other poly(benzimidazole)-containing complexes and to the hemocyanin derivatives. Comparison between the protein's and the complexes' data, support a description of the met-derivatives as a five-coordinated O-bridged binuclear copper(II) center and favors, for both species, a bis(hydroxo) structure with a 3-Å Cu–Cu distance. For *O. vulgaris* met-azido derivative a μ-1,3 bridging mode for the ligand appears the most likely. The structural situation of *C. aestuarii* met-azido-derivative is less clear: a μ-1,1 mode is favored, but a terminal mode cannot be excluded.

INTRODUCTION

Why comparing molluscs and arthropods

Hemocyanins (Hcs) are the oxygen carriers and storage proteins of several species of molluscs and arthropods. Their active site is of a binuclear coupled type with copper ions that are directly bound to six histidine nitrogen atoms of the protein chain. Oxygen is reversibly bound to the active site in a $2Cu:O_2$ ratio as μ-η^2:η^2 peroxide (Solomon et al., 1992; Solomon and Lowery, 1993).

The crystal structures that are available for a 50-kD subunit *Odg* from *Octopus dophlini* (Cuff et al., 1998), for *Panulirus interrupts* (Volbeda and Hol, 1989), and for subunit II of *Limulus polyphemus* (Hazes et al., 1993), allow for a comparison of Hcs from these two phyla. In both cases, the two copper ions in the active site, labeled Cu_A and Cu_B (Ling et al., 1994), are not equivalent and are likely to play a different role in the biological function. The Cu_A copper(II) center that seems to be more accessible to the solvent in the binuclear site controls the reactivity of the site, whereas the second copper(II) center (Cu_B) plays a complex role in controlling the local conformation and electrostatic effects in the oxygenation cycle. An additional difference is observed in the secondary structure elements that include the ligand histidine residues. In the arthropod Hcs, both Cu_A and Cu_B are coordinated by the histidines belonging to a two α-helices motive. In contrast, in the Hcs from molluscs, only the Cu_B is coordinated by a two α-helices motive, whereas the Cu_A is coordinated to one histidine of an α-helix and to two histidines of a loop region, one of which is involved in a unusual thioether bridge.

Also, the comparison of the functional properties of arthropods and mollusc Hcs point out some significant differences that have been documented (van Holde and Miller, 1995 and references therein; Zlateva et al., 1998). The functional properties of the active site are influenced by the protein matrix, which presents different aggregation patterns and different architectures in the two phyla. The arthropod proteins active site is more rigid and less accessible than in molluscan proteins. The greater accessibility in the case of mollusc Hcs allows the protein to exhibit a low-efficiency tyrosinase-like activity involving oxidation of cathecol to quinone.

Chemical reactivity of the Hcs

The binuclear site of the Hcs undergoes, with complex redox chemistry, reactions of exogenous ligands. Small anions and neutral molecules bind to the type 3 Cu site of the Hcs by producing a series of derivatives in which the metallic ions of the active site assume different oxidation states and different coordination geometries. The two copper ions show a different reactivity and the equilibrium position of the ligand substitution reactions depends upon

Submitted October 6, 2001 and accepted for publication November 23, 2001.

Address reprint requests to Elena Borghi, Dipartimento di Chimica, Università "La Sapienza", P. le A. Moro 5, I-00185 Roma, Italy. Tel.: +39-06-4991-3678; Fax: +39-06-490324; E-mail: e.borghi@caspur.it.

0006-3495/02/06/3254/15 $2.00

the type of ligands involved and the pH (Salvato and Beltramini, 1990; Beltramini et al., 1992).

The ligand-binding chemistry occurs with greater affinity in mollusc than in arthropod Hcs and the effects are different. The hydrogen peroxide dismutase activity exhibited by the mollusc Hcs only appears in line with the chemical differences that have been noted between Hc from the two phyla (Himmelwright et al., 1980).

Why met-Hc

The met-Hc form, characterized by an electron paramagnetic resonance-silent [Cu(II) Cu(II)] site, is an important derivative for defining the structural characteristics of the active site in the native protein and to diversify the chemical reactivity of the two Cu sites. The spontaneous, but very slow, reaction of conversion of oxy-Hc to the met-derivative can be stimulated by various anions including fluoride, azide, and acetate (Beltramini et al., 1995 and references therein). The proposed active site model for the met-Hc form assumes a Cu(II) binuclear structure with a di-μ-hydroxo bridge. The pH dependence of the CD features of the met-Hcs and the pH dependence of the azide interaction is suggesting a partial protonation of these bridges at low pH (Beltramini et al., 1995; Alzuet et al., 1997). An extended x-ray absorption fine structure (EXAFS) study (Woolery et al., 1984) shows that there are no differences in the coordination number between the oxy-Hc and met-aquo-Hc forms, however the fundamental question of the origin of the diamagnetism in the met-Hc form is still unresolved.

The binding of azide to met-Hc derivative

Azide is a suitable exogenous ligand for probing the characteristics and accessibility of the active site in various met-Hc derivatives, because, by coordinating with Cu(II), azide produces a complex with a moderate absorption in the 350–440 nm range ($\epsilon \sim 1500$–$2000\ M^{-1}cm^{-1}$) caused by the ligand-to-metal charge transfer (LMCT) transition $N_3 \rightarrow$Cu(II). The absorption and CD LMCT features of this transition (position and intensity) are strongly dependent on the mode of coordination of the ligand anion, thus allowing discriminating between terminal and bridging binding modes of the ligand (Solomon et al., 1992; Solomon and Lowery, 1993).

Concerning azide coordination, *Octopus vulgaris* and *Carcinus aestuarii* met-Hcs differ from each other. The affinity toward azide, the stoichiometry of binding, and its coordination mode show pH dependence. The two met-Hcs exhibit, at pH 7.0, the same 1:1 stoichiometry of the azide adducts. However, the absorption and CD LMCT features suggest that azide binds in a bridging mode in the case of *O. vulgaris* met-Hc active site in contrast to *C. aestuarii* met-Hc where azide binding, probably, occurs on the $Cu(II)_A$ center in terminal mode. The stoichiometry of binding of the azide ligand between the proteins of two phyla differs at pH 5.5. At this pH, a second azide binds to *O. vulgaris* met-Hc. The LMCT features are indicative of a bridging binding mode for the first azide (with greater affinity compared to pH 7.0) and a terminal binding mode for the second azide to copper Cu_A. In contrast, arthropod met-Hc at pH 5.5 binds one azide molecule only.

Assuming the same bis-hydroxo adducts of the binuclear site for both met-Hcs, different reaction models for the binding of azide to *O. vulgaris* and *C. aestuarii* met-Hcs have been proposed (Beltramini et al., 1995; Alzuet et al., 1997). The substitution of the hypothetical exogenous bridging ligands with azide allows for disturbing, in a controlled manner, the structural properties of the binuclear site on the met-Hc forms and for evaluating the effect of different coordination modes of the ligand on the Hcs from the two phyla.

Why x-ray absorption spectroscopy

The synchrotron x-ray absorption spectroscopy (XAS) is an effective technique for selectively investigating the local coordination environment around the metal active site of metalloproteins. The analysis of the oscillations that occur at ~50 eV above the threshold of the x-ray absorption spectrum (EXAFS) provides information on the distances, the number, and the types of atoms surrounding the metal center. The analysis of the threshold region of the spectrum (x-ray absorption near-edge spectroscopy, XANES) provides information on the geometry of the metal–ligand complex. The technique is applicable to samples in any physical state, including liquid or frozen solutions (Hasnain and Hodgson, 1999) and has been successfully used to obtain structural information on the deoxy and oxy-Hc forms, and on other binuclear copper proteins and complexes (Feiters et al., 1999, and references therein; Sabatucci et al., 2002).

A comparative XAS investigation was undertaken to define a more precise structural model for the met- and met-azido oxidized derivatives of *O. vulgaris* and *C. aestuarii* Hcs at pH 7.5 and 5.5. The results presented in this work are restricted to the derivatives at pH 7.5 and to some related mononuclear and binuclear models. Because x-ray data are deposed only for the mononuclear compounds, the XAS characterization of all the related binuclear compounds is of importance. The results concerning the different derivatives at pH 5.5 will be published subsequently (E. Borghi, P. L. Solari, M. Beltramini, L. Bubacco, P. Di Muro, and B. Salvato, unpublished).

MATERIALS AND METHODS

Preparation of the native Hcs and of the Hc derivatives

Native Hcs were isolated from the hemolymph of *O. vulgaris* and *C. aestuarii* and were prepared as described, respectively, in Beltramini et al. (1995) and Bubacco et al. (1992). The protein solutions were stored at −20°C in the presence of 20% (w/w) sucrose as cryoprotectant.

Native Hcs are in equilibrium between the oxygenated and the deoxygenated state that depend on O_2 partial pressure. The conversion to a fully deoxygenated form was achieved under argon atmosphere and was evaluated in a tonometer equipped with a quartz cuvette from the complete disappearance of the band in the absorption spectrum at 345 nm (*O. vulgaris*) and at 340 nm (*C. aestuarii*). A solution of fully oxygenated Hcs exhibits absorbance ratios $A_{345}/A_{278} = 0.25$ (*O. vulgaris*) and $A_{340}/A_{278} = 0.21$ (*C. aestuarii*).

The met-Hc derivative of *C. aestuarii* was prepared by incubating deoxy-Hc (1 mM) with an excess (5 mM) of hydrogen peroxide in 50 mM potassium phosphate buffer at pH 8 at 20°C (Felsenfeld and Prinz, 1959). The preparation of the met-derivative of *O. vulgaris* Hc was also carried out using hydrogen peroxide as described in Zlateva et al. (1998). Azide was added to an *O. vulgaris* deoxy-Hc solution (1 mM) in 50 mM potassium phosphate buffer at pH 6.0 at 20°C, resulting in a final concentration of 100 mM; then the sample was treated with hydrogen peroxide (3 mM) for 20 min. To remove excess reactants, the protein samples of both phyla were dialysed against 50 mM phosphate buffer at pH 7.5. To evaluate the yield of met-Hc, the absorption spectrum of the protein solution was measured. The region around 340 nm is contributed by both the LMCT transitions of met-Hc, whose intensity does not depend on oxygen concentration, and by the peroxide-to-Cu(II) transitions of unreacted oxy-Hc (see above). Thus, recording the spectrum in oxygen and in argon allows the determination of residual oxy-Hc (Zlateva et al., 1998). The met-azido-derivatives of both phyla were prepared by adding mM aliquots of a 1 M buffered solution of the ligand to the met-Hc solution at pH 7.5. For both proteins, the yield of the reaction was evaluated to be more then 95%, according to the residual intensity of the 345-nm band assigned to the unreacted oxy-Hc.

The model compounds

The model compounds used in this study are the mononuclear (Casella et al., 1996) and binuclear (Casella et al., 1993) copper(II) complexes with poly(benzimidazole) ligands, modeling the features of the Cu_2 cores in active site of Hcs.

Two mononuclear complexes of known crystal structure have been considered. These mononuclear compounds are $[Cu(II)(2\text{-}BB)(H_2O)_2](PF_6)_2$ and $[Cu(II)(2\text{-}BB)(N_3)]ClO_4$. The ligand bis[2-(1-methylbenzimidazol-2-yl)ethyl]amine (2-BB), a model of the *tris*(imidazole) array with different coordination numbers and stereochemistries, is related to the L-6,6 ligand (see below).

Six binuclear model complexes $[Cu(II)_2(L)(X)_2](ClO_4)_n$ with L = L-5,5, L-6,6 and X = OH^-, H_2O, N_3^- were prepared as described elsewhere (Casella et al., 1993). The two poly(benzimidazole) ligands α,α'-bis[[bis(1-methyl-2-benzimidazolyl)methyl]amino]-m-xylene (L-5,5) and α,α'-bis[bis[2-(1-methyl-2-benzimidazolyl)ethyl]amino]-m-xylene (L-6,6) have identical donor groups, one tertiary amino and two benzimidazole nitrogen donors, but provide metal coordination sites with different chelate ring size: 5-membered for L-5,5 and 6-membered for L-6,6. Of the six models considered, only the analogous $[Cu(II)_2(L\text{-}5,5)(OMe)_2](ClO_4)_2$ compound has been structurally resolved by x-ray crystallography (Casella, Univ. Pavia, Italy, personal communication).

The XAS measurements

The XAS fluorescence experiments have been carried out at 77 K, in the XANES and EXAFS approaches, on the Italian Collaborating Research Group, General Purpose Italian Beam Line for Diffraction and Absorption at the European Synchrotron Radiation Facility in Grenoble, France. The beam was monochromatized dynamically with two independent Si(311) crystals ($\Delta E/E = 10^{-4}$) (Pascarelli et al., 1996). The dynamical focusing mode avoids solid angle effects during the collection of the fluorescence spectra and produces an intense focal spot on the sample, whose size (~2 mm) is kept constant during each scan. The incident photon flux was measured with an ionization chamber, and the fluorescence photons for each spectrum were collected by using a high-purity germanium multielement detector. Two Pd mirrors were used for harmonic rejection. To avoid radiation damage of the samples, the intensity of incident beam was attenuated with an Al filter of 100 μm.

The energy range used for the detection of the Cu-K_α fluorescence line was 8700–9800 eV for all the spectra. The energy calibration was obtained by measuring, contemporary to the fluorescence signal of a metal copper foil placed after the sample. We collected an average of three to six single scans for each sample with an average integration time of 15 s/point.

The met- and met-azido-derivatives of *O. vulgaris* and *C. aestuarii* Hcs at pH 7.5 were measured in solution in the presence of sucrose. As recently described (Ascone et al., 2000), sucrose provides an excellent protection against x-ray damages, allowing for longer exposure to the x-ray beam. The sucrose was added to the protein solution in a sucrose-to-protein ratio of 50% w/w. The binuclear complexes of the poly(benzimidazole) ligands L-5,5 and L-6,6, and the mononuclear 2-BB model compounds were measured as pellets in 50% w/w sucrose matrix.

Data analysis

The EXAFS first-shell analysis was carried out using the complete package of Michalowicz (1990). To extract the experimental modulation function $\chi(k)$, the free atomic background was reduced by cubic splines using the Heilter formula (Lengeler and Eisenberger, 1980) and normalized to the edge jump.

The $\chi(k)$ function was then multiplied by a Kaiser window before being transformed into real space. The Fourier transforms were obtained by integration of cubic k-weighted EXAFS function over the ~3- to ~11-$Å^{-1}$ range. Structural information was obtained by back-transforming the first peak of the Fourier transform (corresponding to the range 0.8–2.0 Å of the main distance R) and by fitting the resulting function with the appropriate theoretical function defined by Lee and Pendry (1975). This function is expressed in terms of the coordination number N of the first-shell atoms around the photoabsorber atom, in terms of their mean interatomic distance R (Å), and in terms of the variance σ^2 ($Å^2$) (Debye–Waller (DW) factor), which accounts for their structural and thermal disorder. The phase shifts and amplitudes for the photoabsorber and the back-scatterer atoms that were used in the fits were taken from the EXAFS analysis of the Cu K-edge spectra of appropriate reference compounds and from the theoretical data (Mc Kale et al., 1988).

A more detailed quantitative analysis of the EXAFS data has been performed using the GNXAS set of programs (Filipponi et al., 1995; Filipponi and Di Cicco, 1995). The approach with the GNXAS package involves an ab initio calculation of the absorption coefficient cross-section using the multiple-scattering theory, starting from a given geometrical atomic configuration around the absorber. The theoretical structural signal $\chi(k)$ is calculated as a sum of the two-body single scattering signal (SS) and the three-body and four-body multiple scattering signals (MS) associated with the n-atom configurations including the photoabsorber. The two-body signals are associated with pairs of atoms and probe their distances and variances. The three-body signals are associated with triplets of atoms and probe angles and their variances. The four-body signals are associated with quartet of atoms and probe the presence of the imidazole rings of a

histidine residue (protein case) or of a benzimidazole residue (model case) (Meneghini and Morante, 1998). Then, by comparison with experimental data, the model signal is refined with a fitting procedure.

In both approaches, the statistical errors associated with the parameters were calculated by assuming that the residual is a χ^2-distributed variable and by considering a critical value corresponding to the 95% confidence level (Michalowicz, 1990; Filipponi and Di Cicco, 1995).

The near-edge structure (XANES) spectra were normalized to the total jump after removal of a linear background. The background was fitted in the pre-edge region and extrapolated to the whole spectrum. In all spectra, the zero on the energy scale was fixed at 8979.0 eV, corresponding to the first inflection point of the absorption threshold of metal copper.

RESULTS AND DISCUSSION

The XAS investigation of binuclear copper sites as those found in Hcs poses some severe problems that mainly derive from the presence of two scattering atoms and from the fact that the metal–metal contribution in the spectra is superposed to the Cu-His signals. The determination of both a correct value of the Cu–Cu distance and a measure of the apical distortion at the copper site, considering that the apical histidine movement is certainly involved in the mechanism of ligand association, are the two fundamental aspects that we are aiming to resolve with this investigation.

To evaluate the accuracy of our analysis, we considered, as a first test, the two mononuclear model complexes with resolved x-ray crystallographic structures. In the aquo complex, the metal center is five-coordinated in a compressed trigonal bipiramidal stereochemistry. In the azido complex, the metal center is four-coordinated in a stereochemistry intermediate between square planar and tetrahedral. The azide ligand is bound in an end-on coordination mode with the two N–N bonds statistically equal.

The following step has been to consider the L-5,5-$(OH)_2$ binuclear model. Also, for this complex, a resolved x-ray structure is available, and so it constitutes a test for the accuracy of our analysis in the presence of a binuclear metal site. The L-5,5 complex is a good model for the proposed bis(hydroxo)-bridge structure of the binuclear copper(II) center in the met form of the protein. In fact, the L-5,5 ligand complex, which constrains the chelation on each Cu(II) center with two five-term rigid rings, presents an antiferromagnetic coupling as in the met-Hc form. The L-6,6 bis(hydroxo)di-Cu(II) complex, which has also been considered, has a higher flexibility that is more apt to mime the redox reactivity of the protein. Thus, the study of this complex is useful to evidence small differences of the coordination geometry that occur in the site and, in particular, the movements of the apical ligand. Of the other models that we have considered, the two bis(aquo)di-Cu(II) complexes may provide the basis to identify the differences between a bis(hydroxo)-bridge and a bis(aquo)-bridge structure to test the possibility that the bridging ligand in the Hcs derivatives is a water molecule. The two bis(aquo) complexes show a high affinity for the azide and differentiate the mode in which the azide ligand is coordinated. Finally, the two monoazide adducts of the binuclear derivatives have been considered because they show a μ-1,3 bridging coordination for L-6,6 and a μ-1,1 for L-5,5. Their features, and those of the azido-mononuclear complex, provide information on the three possible coordination modes of the azide ligand. The complete MS analysis of all the models considered will be published in a separate article. In this study, we are reporting only the XAS results of the model compounds that are important for the comprehension of the analogous characteristics of the related biological samples. Confident in the validity of this approach, which gives results that are in agreement with previous spectroscopic studies (see below), we have extended the XAS analysis to the Hcs derivatives.

EXAFS approach

In Figs. 1–4, we show the cubic *k*-weighted Cu K-edge EXAFS (*A parts*) and Fourier transforms (FTs) (*B parts*) for the met- and met-azido Hc forms of the two species considered (Fig. 1), for the binuclear L-5,5 models (Fig. 2), for the binuclear L-6,6 models (Fig. 3), and for the mononuclear 2-BB models (Fig. 4).

In the FTs (*part B* of Figs. 1–4), the intense first peak is assigned to the scattering from the nearest neighbor atoms. The following secondary peak of variable amplitude is assigned primarily to the scattering from the second shell of atoms of the histidine imidazole rings and partially to the Cu–Cu scattering. The third peak is due primarily to the external shell of atoms of the imidazole rings. By comparing the different FT spectra, we observe significant differences among the various compounds on going from the hydroxo-, to the aquo-, and to the azide form. In the L-5,5 FT spectrum (Fig. 2 *B*), the first and second peak decrease. In the L-6,6 FT spectrum (Fig. 3 *B*), the decrease of the first peak is more pronounced and the following peaks increase. The same trend is observed with the mononuclear compounds (Fig. 4 *B*). The decrease of the FT first peak is much smaller in the case of met- and met-azido-Hcs as compared to the models (Fig. 1 *B*). The binding of azide to met-Hc produces little changes at ~3.0 Å (*Carcinus* case) and between 2.0 and 3.0 Å (*Octopus* case).

The first-shell analysis

The FT first-shell peaks were filtered, back-transformed, and analyzed for nearest neighbors scattering atoms. At this stage of the analysis, it was not possible to separate the contributions of the different low Z atoms (N/O) due to the high correlations that exist between the parameters of the subshells. The values obtained in the fits are shown in the left side of Table 1. The errors are given in parentheses and refer to the last digit of the parameters. These results indicate that, for all the samples, a single shell of low Z atoms at an average distance of 1.94–1.98 Å can be considered.

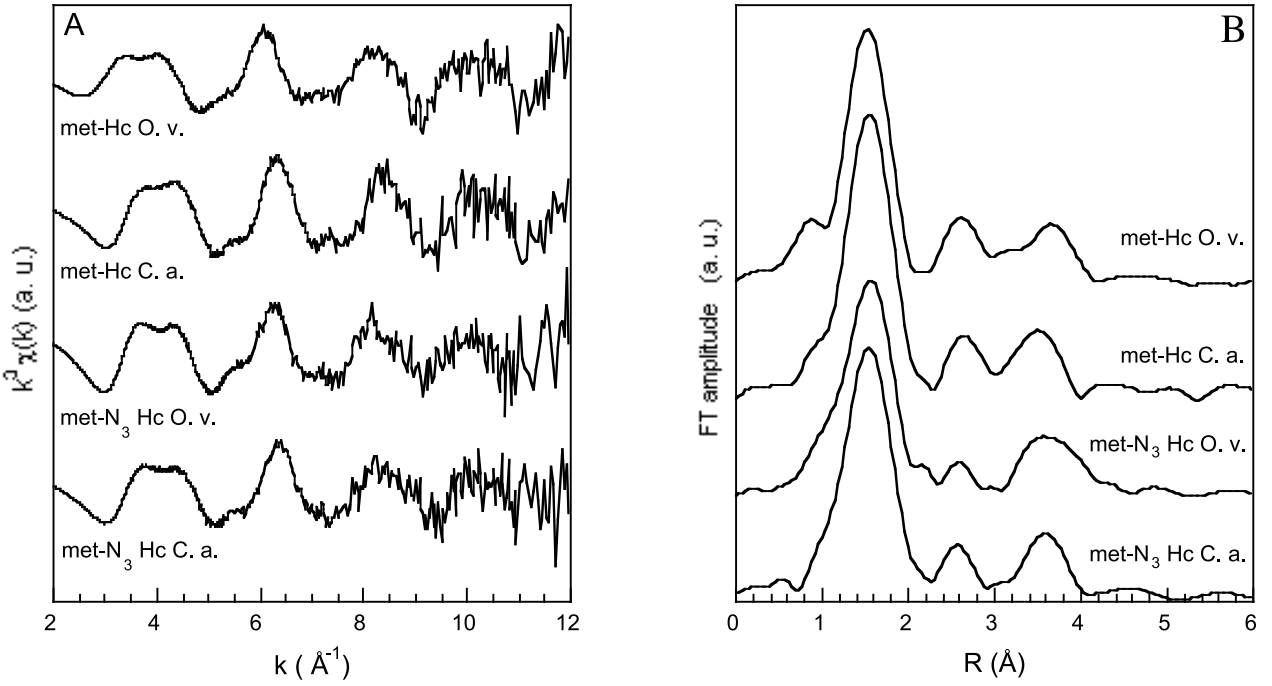

FIGURE 1 Comparison of the (*A*) cubic *k*-weighted EXAFS and of the (*B*) corresponding Fourier transforms for the met-Hc and met-azido-Hc derivatives from *O. vulgaris* and *C. aestuarii*.

Of the three models with a resolved structure, only the results obtained for the 2-BB-N_3 are consistent with the crystallographic data (4-coordination at an average distance of 1.94 Å). Indeed, for the 2-BB-$(H_2O)_2$ and the L-5,5-$(OH)_2$ compounds, the coordination numbers are apparently dissimilar with the known structures (3- and 4-coordinated instead of 5-). This discrepancy may be acceptable if one considers the experimental error associated with the coordination number (see Table 1, *left side*). However, more probably, the results are a consequence of the inability of the first shell Fourier filter analysis to account for the presence of the distal first-shell-coordinating atoms: the two oxygens in the case of 2-BB-$(H_2O)_2$ and the apical nitrogen (i.e., the tertiary amino donor) in the case of the L-5,5-

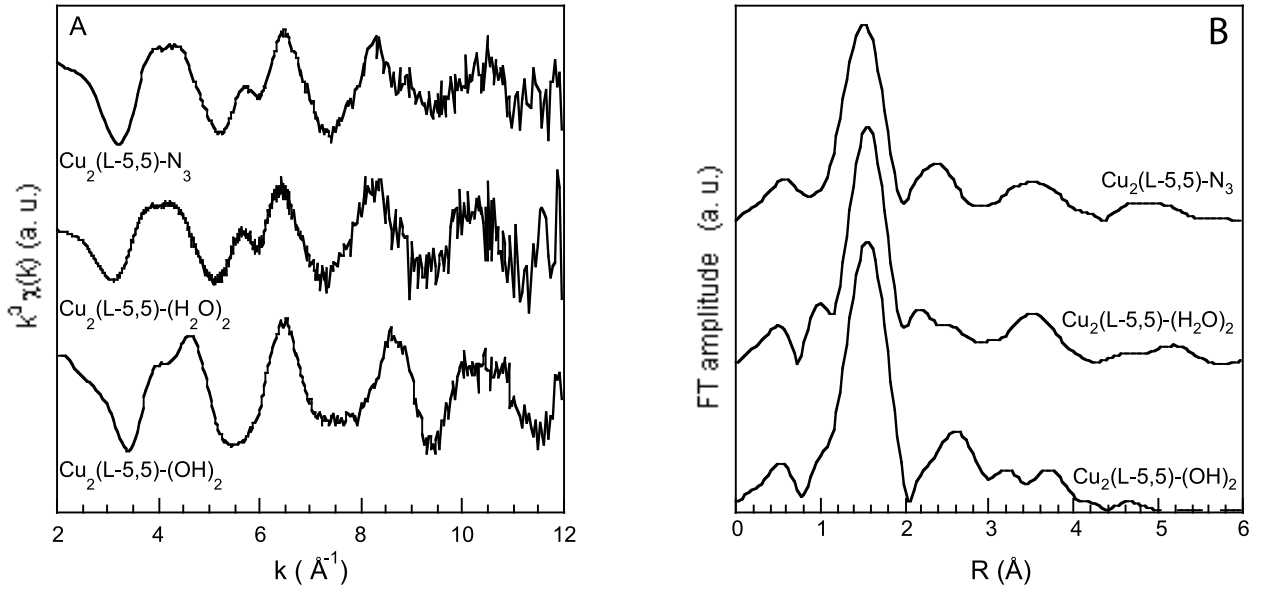

FIGURE 2 Comparison of the (*A*) cubic *k*-weighted EXAFS and of the (*B*) corresponding Fourier transforms for the $[Cu_2(L\text{-}5,5)(X_2)](ClO_4)_n$ complexes with $X = OH^-$, H_2O, N_3^-.

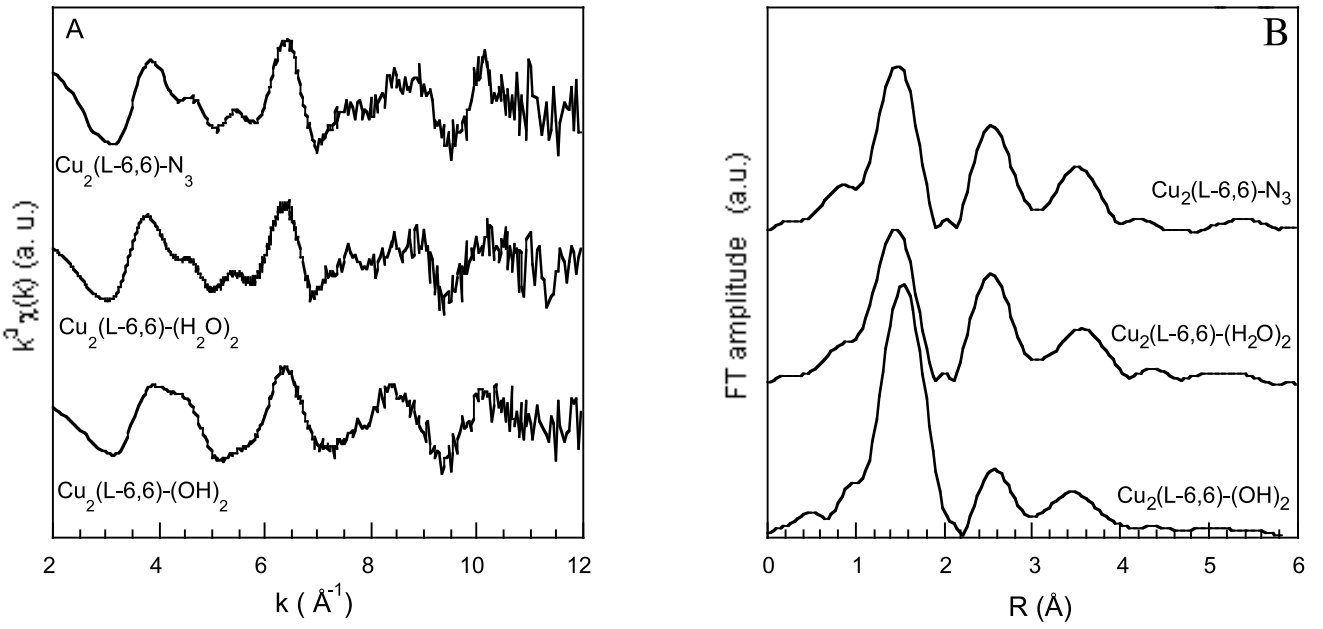

FIGURE 3 Comparison of the (*A*) cubic *k*-weighted EXAFS and of the (*B*) corresponding Fourier transforms for the $[Cu_2(L\text{-}6,6)(X_2)](ClO_4)_n$ complexes with $X = OH^-$, H_2O, N_3^-.

$(OH)_2$ (Fonda et al., 2001; Casella et al., 1996; L. Casella, Univ. Pavia, Italy, personal communication).

The values obtained for the models of both families indicate that the decrease observed in the first FT peak, on going from the hydroxo- to the aquo- and to the azide-form (Figs. 2 *B* and 3 *B*), is the result of a combined decrease of the coordination number and increase of the Debye–Waller factor. The decrease of the coordination number can be explained, at least in part, by the displacement of some coordinating atoms to distal positions. The trend seen for the DW factors is in agreement with an expected increase of the static structural disorder around the metal center.

The results obtained for the Hcs indicate fine differences between the met- and met-azido-forms (see Table 1, *left side*). The *O. vulgaris* Hc appear to have a slightly longer first shell average distance and a slightly greater DW factor with respect to the *C. aestuarii* Hc, thus having a greatly disordered active site.

The multiple-scattering approach

Although the Fourier filtering in the single-scattering approach is a suitable method to investigate the first shell, it gives unreliable results for the analysis of the subsequent

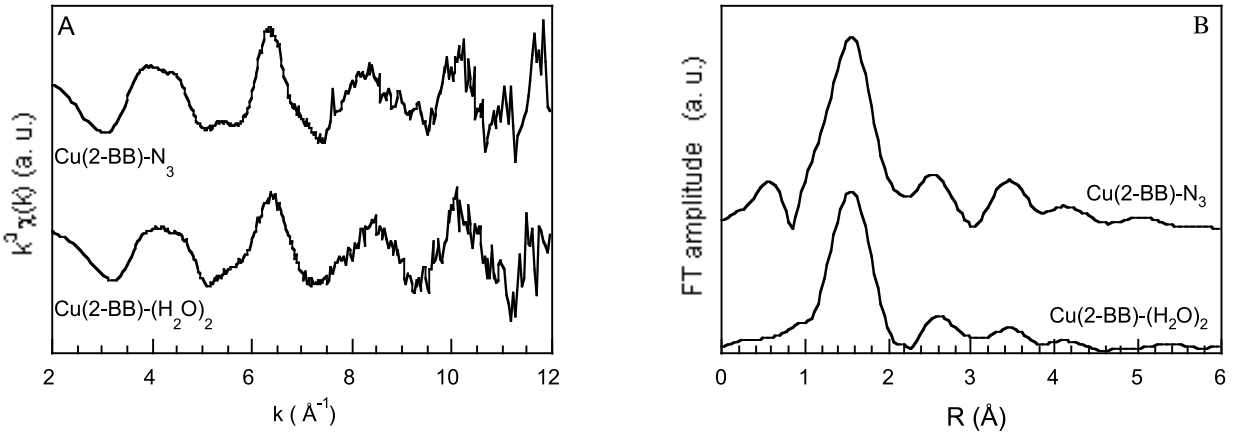

FIGURE 4 Comparison of the (*A*) cubic *k*-weighted EXAFS and of the (*B*) corresponding Fourier transforms for the $[Cu(2\text{-}BB)(H_2O)_2](PF_6)_2$ and $[Cu(2\text{-}BB)(N_3)]ClO_4$ complexes.

TABLE 1 Results of the EXAFS single-scattering Fourier filter method for the first shell and of the EXAFS multiple scattering analysis for the whole spectrum

	Single Scattering Analysis First Shell			Multiple Scattering Analysis			
Sample	*N*	R (Å)	σ^2 (Å^2)		*N*	R (Å)	σ^2 (Å^2)
$[Cu(2\text{-}BB)(H_2O)_2](PF_6)_2$	2.8 (6)	1.97 (2)	0.003 (1)	Cu-N	2	1.97 (2)	0.002 (1)
				Cu-O′distal	2	2.40 (5)	0.038 (5)
				Cu-N′axial	1	2.01 (3)	0.002 (2)
$[Cu(2\text{-}BB)(N_3)]ClO_4$	4.0 (7)	1.94 (2)	0.006 (2)	Cu-N	4	1.96 (2)	0.003 (1)
$[Cu_2(L5,5)(OH)_2](ClO_4)_2$	4.1 (6)	1.95 (2)	0.004 (1)	Cu-O	2	1.94 (1)	0.0010 (7)
				Cu-N	2	1.95 (2)	0.003 (1)
				Cu-N′axial	1	2.55 (3)	0.006 (2)
				Cu-Cu	1	3.04 (1)	0.0110 (6)
$[Cu_2(L\text{-}5,5)(H_2O)_2](ClO_4)_4$	3.2 (8)	1.97 (3)	0.004 (2)	Cu-O	1	1.97 (2)	0.001 (1)
				Cu-N	2	1.98 (1)	0.003 (2)
				Cu-O′distal	1	2.10 (3)	0.010 (3)
				Cu-N′axial	1	2.37 (2)	0.006 (3)
				Cu-Cu	1	3.33 (6)	0.012 (3)
$[Cu_2(L\text{-}5,5)(N_3)(H_2O)](ClO_4)_3$	3.5 (6)	1.96 (1)	0.008 (1)	Cu-O	1	1.96 (3)	0.006 (5)
				Cu-N	2	2.02 (3)	0.002 (1)
				Cu-Nazide	1	1.91 (2)	0.003 (1)
				Cu-N′axial	1	2.2 (1)	0.013 (6)
				Cu-Cu	1	3.19 (7)	0.014 (6)
$[Cu_2(L\text{-}6,6)(OH)_2](ClO_4)_2$	4.0 (6)	1.96 (2)	0.005 (1)	Cu-O	2	1.917 (8)	0.002 (1)
				Cu-N	2	2.02 (1)	0.003 (2)
				Cu-N′axial	1	2.34 (5)	0.01 (1)
				Cu-Cu	1	2.99 (2)	0.006 (2)
$[Cu_2(L\text{-}6,6)(H_2O)_2](ClO_4)_4$	3.2 (5)	1.96 (2)	0.010 (1)	Cu-O	1	1.91 (2)	0.003 (3)
				Cu-N	2	1.96 (1)	0.003 (2)
				Cu-O′distal	1	2.084 (8)	0.004 (2)
				Cu-N′axial	1	2.22 (2)	0.005 (3)
				Cu-Cu	1	2.93 (2)	0.007 (2)
$[Cu_2(L\text{-}6,6)(N_3)(H_2O)](ClO_4)_3$	3.0 (5)	1.95 (2)	0.009 (1)	Cu-O	1	1.901 (6)	0.002 (2)
				Cu-N	2	2.042 (5)	0.003 (1)
				Cu-Nazide	1	2.23 (1)	0.003 (3)
				Cu-N′axial	1	2.38 (2)	0.007 (6)
				Cu-Cu	1	3.77 (7)	0.01 (1)
Octopus vulgaris met-Hc	4 (1)	1.97 (3)	0.005 (2)	Cu-O	2	1.964 (8)	0.003 (1)
				Cu-N	2	1.94 (1)	0.010 (2)
				Cu-N′axial	1	2.38 (3)	0.011 (4)
				Cu-Cu	1	3.01 (2)	0.006 (3)
Octopus vulgaris met-N_3 Hc	4 (1)	1.98 (3)	0.006 (1)	Cu-O	1	1.86 (1)	0.003 (2)
				Cu-N	2	2.000 (7)	0.001 (1)
				Cu-Nazide	1	2.07 (2)	0.003 (2)
				Cu-N′axial	1	2.31 (3)	0.008 (7)
				Cu-Cu	1	3.80 (4)	0.005 (5)
Carcinus aestuarii met-Hc	4 (1)	1.96 (2)	0.004 (1)	Cu-O	2	1.91 (1)	0.006 (1)
				Cu-N	2	1.97 (1)	0.001 (1)
				Cu-N′axial	1	2.37 (5)	0.008 (7)
				Cu-Cu	1	2.98 (4)	0.008 (5)
Carcinus aestuarii met-N_3 Hc	4 (1)	1.95 (3)	0.005 (1)	Cu-O	1	1.90 (1)	0.005 (3)
				Cu-N	2	1.985 (9)	0.007 (3)
				Cu-Nazide	1	2.00 (2)	0.005 (3)
				Cu-N′axial	1	2.32 (2)	0.011 (3)
				Cu-Cu	1	3.20 (3)	0.020 (1)

shells. Indeed, outside the first-shell range, the multiple scattering contributions from the imidazole rings that surround the metal center become particularly important. Therefore, we have started an analysis of the whole spectra with the multiple-scattering approach using the GNXAS package programs (Filipponi et al., 1995; Filipponi and Di Cicco, 1995).

From the MS analysis performed on the compounds and on the Hcs derivatives, the trend described above for the first-shell analysis seems to be confirmed. In the right side of Table 1, we report the results (with errors in parentheses) obtained by distinguishing two, three, or four different waves for the first shell (the Cu–O, the equatorial Cu–N, the apical Cu–N′, and a second Cu–O or Cu–N shell for the aquo- and the azido-compounds, respectively). The low coordination numbers observed in the Fourier-filter first-shell analysis appear effectively to be a consequence of the longer distances of some of the first neighbors or of the greater value of the Debye–Waller factors associated with some of the subshells.

In Table 1, we also report the first results obtained for the Cu–Cu shell. It is known (Scott and Eidsness, 1988) that, in biological systems and biomimetic models involving heterocyclic aromatic ligands (imidazole, pyridine), it may be a problem to distinguish the Cu contribution from low-Z (C/N in second and third shells) contributions at the same distance, because the contributions are different only in the envelope of the backscattering amplitude, while the phase relationships between EXAFS and FT are the same. By using a multiple scattering-fit approach, it becomes possible to establish the Cu–Cu distance (Lynch et al., 1994; Feiters et al., 1999), but, nonetheless, this remains a difficult task.

The results obtained for the mononuclear compounds and for the L-5,5-$(OH)_2$ are in agreement with the structural data. Only for the 2-BB-aquo is there a slight increase of the average distance of the coordinating waters, which can be partly attributed to the strong disorder associated with these atoms.

The results obtained for the L-6,6-$(OH)_2$ are comparable to those of the L-5,5-$(OH)_2$. The L-6,6 bis(hydroxo) complex is characterized by a shorter apical ligand distance. The shorter distance obtained for the apical nitrogen and the longer average distance obtained for the equatorial nitrogens are in agreement with the lower conformational rigidity imposed by the L-6,6 poly(benzimidazole) ligand. The XAS values indicate that the binuclear copper(II) centers with the two ligands show a similar bis(hydroxo)-bridged structure (i.e., similar Cu–Cu distance, similar coordination number in the first shell) so that a similar geometry of the overall cluster is expected. This agrees with previous spectroscopic studies (Casella et al., 1993).

For the L-5,5-$(H_2O)_2$, the data can be fitted correctly only by separating the contribution of the oxygens of the two water molecules. We find that one of the oxygens is displaced at a larger distance with respect to the bis(hydroxo) form. This agrees with the Fourier filter analysis for which a reduction of coordination number of the first neighbors was observed. The observed variation in the Cu–Cu distance, besides the Cu–O/O′ and the Cu–N/N′ distances, comports a perturbation in the Cu–O–Cu angle, so a different symmetry of the Cu cluster is expected, as compared to the bis(hydroxo) complex. The same effect is seen for the L-6,6-$(H_2O)_2$ compound with respect to the L-6,6-$(OH)_2$ one. The shorter Cu–Cu distance in this case reflects the presence of a more ordered geometry consistent with the L-6,6 ligand-forming six-membered chelate rings instead of five-membered as with L-5,5 ligand.

The L-5,5-N_3 spectra can be adequately fitted, including one oxygen and three equatorial nitrogens (one is coming from the azide) at an average distance of ~1.9 Å. An additional axial nitrogen at 2.2 Å, which takes into account the contribution of the apical Cu-N′ of the L-5,5 ligand, has to be considered. The best fit was obtained by starting the calculations from a theoretical model, which accounts for the L-5,5 geometry of the ligand and for the μ-1,1 bridging coordination of the azide (as in the model by Kahn et al., 1983). The first-shell coordination, the MS results obtained and the average Cu–Cu distance (~3.20 Å) indicate a different geometry of the copper cluster as compared to the bis(hydroxo) complex and are compatible with the presence of the μ-1,1 azide-bridged structure.

For the L-6,6-N_3, the best fit is obtained by considering an azide contribution in the μ-1,3 bridge coordination. The first shell is correctly fitted by two equatorial nitrogens at ~2 Å and one oxygen. The contributions coming from the nitrogen of the azide and from the ligand are found at larger distances. The long distance obtained for the Cu–Cu shell is compatible with the (μ-hydroxo)(μ-1,3-azido) model of Kitajima et al. (1993), which shows similar distances (average Cu–N at 2.02 Å, Cu–N at 2.21 Å). The distance obtained for the oxygen atom is compatible with the second aquo bridge expected in this adduct (Casella et al., 1993). As we already stressed, the results obtained on the model compounds that are presented in this work are used as a proof of the goodness of our approach, and they will be discussed in detail elsewhere.

The results of the fits of the EXAFS of the Hcs forms, obtained with the multiple scattering approach are shown in Fig. 5. The best fit value of the residual, R_{exp}, and the calculated expected value, R_{th}, (Filipponi and Di Cicco, 1995) are also shown in the figure as a measure of the goodness of the fits. The differences between the met- and met-azido Hcs forms of the two phyla, which are less evident in respect to those noted for the models when considering the first-shell analysis, can be partly clarified by the MS approach. In all cases, the two derivatives of both species are five-coordinated and the distances of the first-shell atoms are included between 1.9 and 2.0 Å (see Table 1).

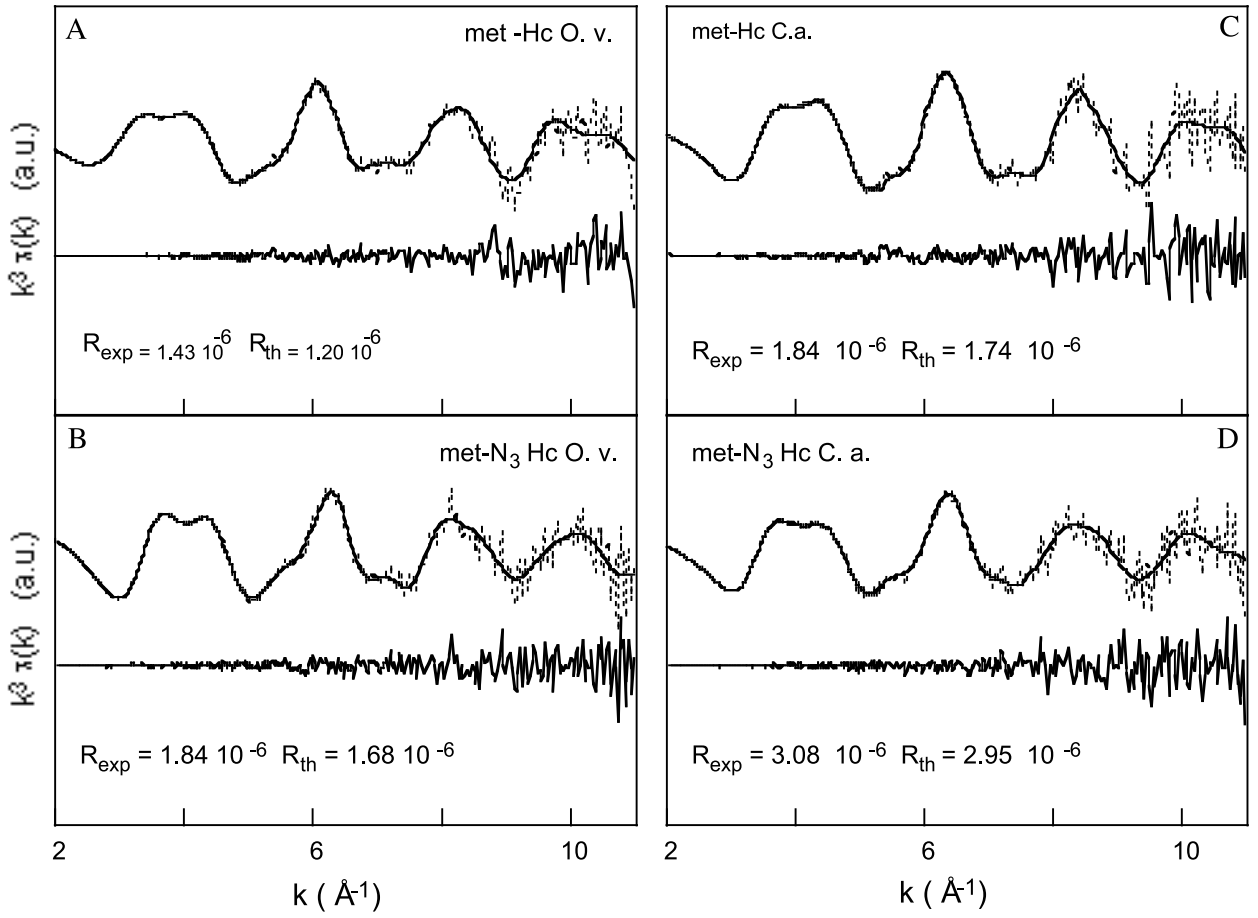

FIGURE 5 Results of the best fits of the cubic *k*-weighted EXAFS for (*A*) met-Hc and (*B*) met-azido-Hc derivatives from *O. vulgaris* and for (*C*) met-Hc and (*D*) met-azido-Hc derivatives from *C. aestuarii*. The total simulated signals (*continuous line*) are superimposed on the experimental signals (*dotted line*). At the bottom of panels the residual functions are plotted. The values of R_{exp} and R_{th} are reported.

For the met-Hcs, the best fits were obtained by considering as a starting structure the met-form of *Limulus polyphemus* Hc (1LL1 PDB-record), which presents a Cu–Cu distance of 3.127 Å and an average bending angle (Cu–O–Cu) of ~102° (Fig. 5, *A* and *C*). The results obtained in this study are consistent with a five-coordination number as is the case for the oxy-Hc (Feiters, 1990). In effect, by distinguishing between the Cu–O wave and the Cu–N equatorial and Cu–N′ apical waves coming from the imidazole, the met-Hc forms appear three-coordinated with the nitrogen atoms and two-coordinated with the oxygen. The apical nitrogen is found for both proteins at an average distance of 2.3–2.4 Å, which is close to the value found for the L-6,6-$(OH)_2$ compound. For both species, a shorter Cu–Cu distance, of ~3 Å, is obtained with respect to the oxy-Hc, in which the oxygen is coordinated in the μ-η^2:η^2 mode, and the Cu–Cu distance is ~3.5 Å. By itself, the shorter Cu–Cu distance could account for the magnetic coupling of the type 3 site of the met derivatives without the necessity of invoking additional bridging ligands. Nevertheless, the results obtained with the model compounds show that a double O coordination at a distance of 1.95 Å or lower, and a short Cu–Cu distance at ~3.0 Å, are expected in the case of a bis(hydroxo) structure, whereas the results seem to be incompatible with bis(aquo) structure, for which longer distances are obtained for one of the two water molecules. Thus, our results, in which the Cu–O–Cu multiple-scattering path has been considered, seem to assert the presence of a bis(O)-bridged structure and are consistent with a perturbation of the bending angle of the Cu_2O_2 unit to a value of ~100–102°. (Note that it is ~137° in the oxy case [Cuff et al., 1998 and references therein]). Also the EXAFS calculations by Feiters et al. (1999) for O_2 complexes with the Cu–Cu parameters at the same distance indicate a similar bending. A Cu–Cu distance ~3 Å in the met-Hcs forms is also concordant with the trend that is seen for Cathecol oxidases, in which the Cu–Cu distance decreases from 3.8 to 2.9 Å upon going from the oxy- to the met-form, though, in this later case, a decrease in the coordination has also been observed (Eicken et al., 1998). Compared to the model

compounds that we have considered, the results for the met-Hcs forms appear to be similar to those obtained for the L-6,6-bis(hydroxo) complex. This similarity and the differences obtained with respect to a previous work on different Hc phyla, in which met-aquo forms were considered (Woolery et al., 1984), favors the hypothesis of the hydroxide atoms as exogenous ligands for the met-Hc forms.

Using the MS approach, the results obtained for met-azido-Hcs bring up differences between the derivatives of the two species that were not detectable by a simple first-shell analysis (Fig. 5, *B* and *D*). The azide-derivatives are also different with respect to their met-correspondent, though, maybe, to a lesser extent than what is observed for their homologous model compounds.

The starting spectroscopic hypothesis for the azide-binding mode is an end-on geometry for *C. aestuarii* derivative (Alzuet et al., 1997) and a μ-bridge geometry for *O. vulgaris*, with a preferred μ-1,3 bridging mode (Beltramini et al., 1995). For the *O. vulgaris* met-azido-Hc, the best fits were obtained by considering a structure with a coordinated μ-1,3 azido bridge as the starting model for the calculations of the theoretical signal (Fig. 5 *B*). The results indicate that the protein is five-coordinated with a longer Cu–Cu distance, of ~3.8 Å. The shorter value obtained for the Cu–O distance may indicate a severe distortion of the Cu–O–Cu bridge or probably the breaking of this bridge, each copper being coordinated to a different oxygen atom. Nonetheless, the proposed μ-1,3 bridging coordination mode for the azide is the most favorable, because alternative fits starting from μ-1,1 bridging coordination were unsatisfactory. So, in this case, the spectroscopic hypothesis seems to be confirmed.

For the *C. aestuarii* met-azido-Hc, the best fits were obtained by considering a μ-1,1 bridging structure as the starting model for the calculations (Fig. 5 *D*). In this case, the differences in the first shell between the azide derivative and the met derivative are less important. The protein is five-coordinated and the Cu–Cu distance is ~3.2 Å as for the L-5,5-N_3 complex. However, the starting hypothesis for the *Carcinus* case is an end-on geometry, the first shell and Cu–Cu shell results seem to favor a μ-1,1 bridging mode. The results obtained in a previous EXAFS study, in which the MS contributions where not considered (Woolery et al., 1984), suggested a μ-1,3 geometry, with a Cu–Cu distance of ~3.7 Å, for both molluscan and arthropodan Hcs. This cannot be in our case for the *Carcinus* derivative.

XANES approach

Figures 6–9 show the normalized XANES spectra (*upper panels*) and the relative first derivatives (*lower panels*) of the met- and met-azido-Hcs and of the poly(benzimidazole) compounds. The energy position of the Cu K-edge for all the considered model complexes and protein derivatives is

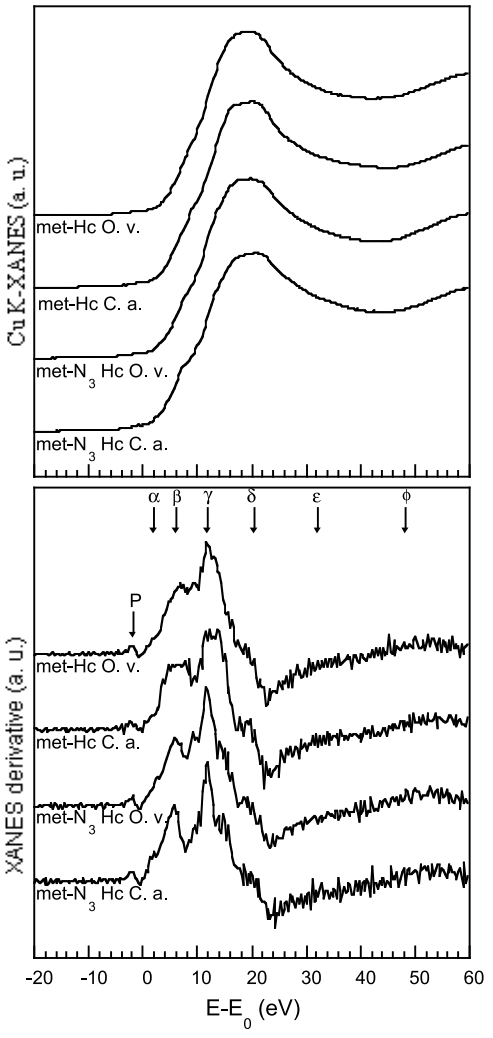

FIGURE 6 Comparison of the Cu K-edge XANES spectra (*upper panel*) and of the corresponding XANES derivative spectra (*lower panel*) for the met-Hc and met-azido-Hc derivatives from *O. vulgaris* and *C. aestuarii*. In the derivative spectrum the features (P, α, β, γ, δ, ϵ, φ) are shown.

in the range of the $3d^9$ electronic configuration of Cu(II) with N/O donors coordination. All the spectra show features in the pre-edge region, in the rising-edge region and in main-peak region, which have been detected and assigned for other Cu(II) clusters (Kau et al., 1987; Sano et al., 1992; Shadle et al., 1993, Pickering and George, 1995). Because the XANES spectra are expected to contain significant information on each copper-site symmetry, the position and the intensity of the XANES features can be correlated to general geometric properties of the metal site to elucidate qualitatively some aspects of the copper-site conformational changes. Our qualitative discussion of the low-energy region of XAS spectra will refer to the meanings of the experimental XANES features and to the information obtainable from the MS simulations of the XANES spectra reported in literature for Cu(II) complexes with coordination through N/O donors.

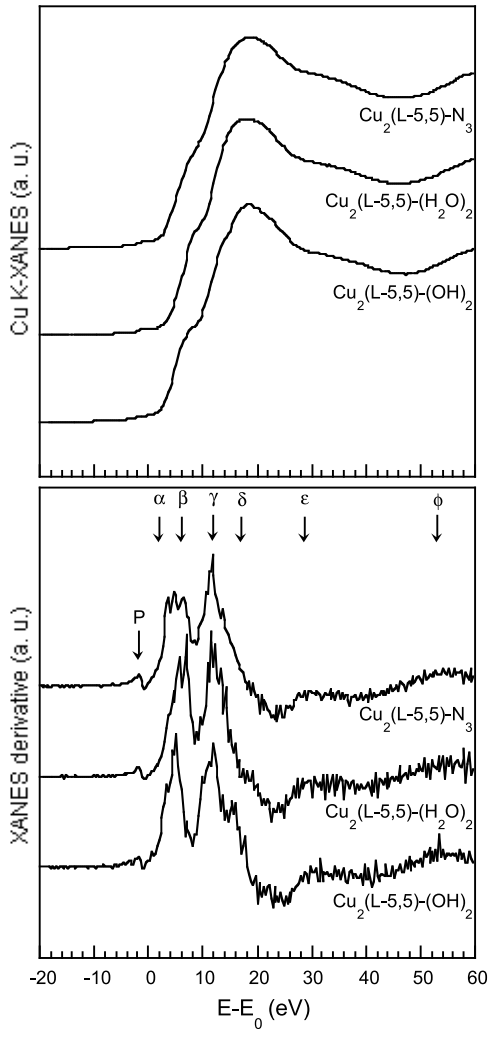

FIGURE 7 Comparison of the Cu K-edge XANES spectra (*upper panel*) and of the corresponding XANES derivative spectra (*lower panel*) for the $[Cu_2(L\text{-}5,5)(X_2)](ClO_4)_n$ complexes with $X = OH^-$, H_2O, N_3^-. In the derivative spectrum the features (P, α, β, γ, δ, ϵ, φ) are shown.

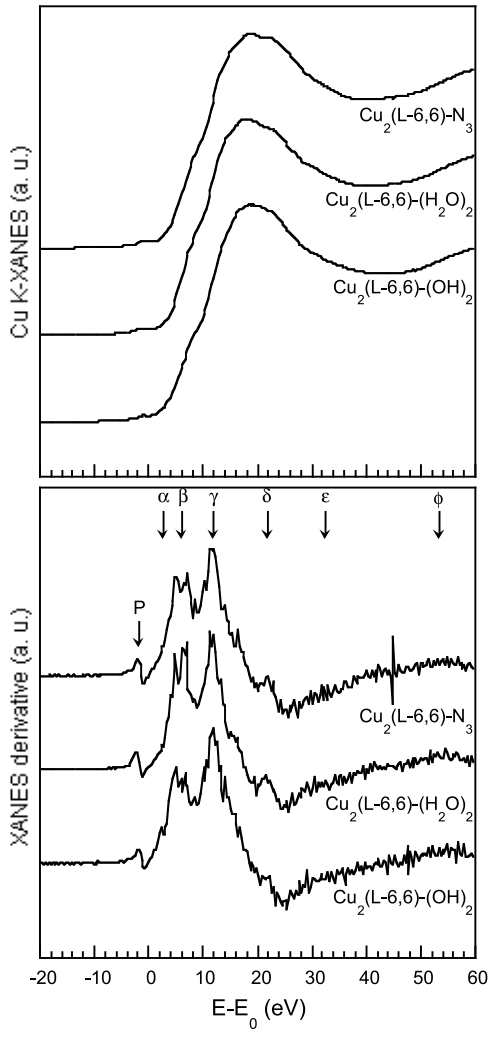

FIGURE 8 Comparison of the Cu K-edge XANES spectra (*upper panel*) and of the corresponding XANES derivative spectra (*lower panel*) for the $[Cu_2(L\text{-}6,6)(X_2)](ClO_4)_n$ complexes with $X = OH^-$, H_2O, N_3^-. In the derivative spectrum the features (P, α, β, γ, δ, ϵ, φ) are shown.

Meaning of the XANES features

The pre-edge P feature corresponds to the formally dipole-forbidden 1s→3d transition ($\Delta l = \pm 2$, quadrupole allowed, l being the azimuthal quantum number). The presence of the P feature (the smallest resolved feature in the spectrum at the energy absorption ≈ 0 eV) marks the copper valence state as Cu(II). The intensity of the P feature for Cu(II) complex depends, mainly, on the centro-symmetric character of the average symmetry around the Cu(II) metal. This peak is absent for centro-symmetric clusters in which the 1s→3d transition is completely dipole forbidden, but has a nonzero intensity for noncentro-symmetric clusters and raises to a strong intensity for tetrahedral clusters due to the metal d–p orbital mixing through the perturbation of the ligand field. So differences in the pre-peak P intensity are reflecting different average symmetry around the Cu(II) center (Sano et al., 1992).

The A, B, C, D features, labeled in order of increasing energy, and their related α, β, γ, δ peaks in the first derivative spectra are typical of the Cu K-edge and correspond to the electric dipole-allowed 1s→4p transition ($\Delta l = \pm 1$). The two higher-energy features E, F (and the related derivative peaks ϵ, φ), which intensities are relatively low in comparison to those of the features at lower energies, may not be accurately estimated.

The 1s→4p transition and the corresponding creation of the core hole cause a relaxation of the valence levels. Two final states are possible: the $(1s)^1\cdots(3d)^9 4p^1$ configuration associated with the pure 1s→4p transition (main resonance peak) and the $(1s)^1\cdots(3d)^{10}L^{-1}4p^1$ configuration (where L^{-1} denotes a copper ligand hole) associated with the two-electron 1s→4*p* + LMCT transition (shakedown resonance peak). The ligand-to-metal charge-transfer energy shifts the shakedown resonance to a lower energy. At

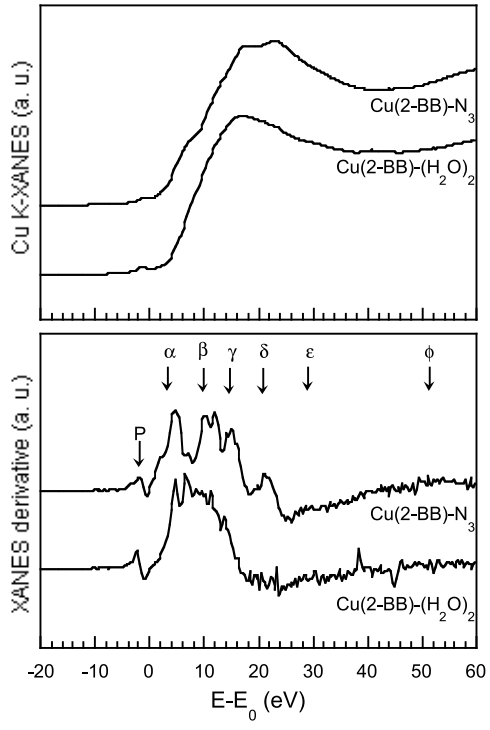

FIGURE 9 Comparison of the Cu K-edge XANES spectra (*upper panel*) and of the corresponding XANES derivative spectra (*lower panel*) for the $[Cu(2\text{-}BB)(H_2O)_2](PF_6)_2$ and $[Cu(2\text{-}BB)(N_3)]ClO_4$ complexes. In the derivative spectrum the features (P, α, β, γ, δ, ϵ, φ) are shown.

present, the typical near-edge A-to-D structures are believed to be two replicas of the same one-electron and two-electron transitions, i.e., the A and C features are assigned to the shakedown transition and B and D are assigned to the main transition (Shadle et al., 1993; Pickering and George, 1995).

The A and B features are the peaks in the rising-edge region. The A feature (peak α) at the absorption edge (A, 4–7 eV) is originated by the tetragonal distortion in the metal cluster, and its magnitude and position depend on the degree of the distortion. This structure is absent for centrosymmetric six-fold coordinated clusters, but it is present as a shoulder for a moderate tetragonal distortion or as a broad band for a square planar symmetry (Palladino et al., 1993; Pickering and George, 1995). The A feature is also expected with T_d and C_{3v} symmetry clusters, and a not negligible presence of this feature has been suggested to be an indicator of a five-fold square-pyramidal coordination (Della Longa et al., 1993). It has been shown (Kau et al., 1987) that its intensity is in the 0.15–0.5 values range for Cu(II) clusters. Also, the B feature (peak β) (B, 8–14 eV) reflects essentially the difference in the axial geometry of the Cu clusters.

The C and D features occur in the main peak region. The C feature (peak γ) is at 14–19 eV, whereas the D structure (peak δ) is at 18–22 eV. These features reflect the coordination number and the symmetry of the Cu sites. The presence of well-distinct features in this region can be an indicator of an anisotropic character due to inequivalence on the coordination geometry of p_x, p_y, p_z orbitals. The features at higher energy E (20–30 eV) and F ($\geq$30 eV), when of observable intensity, are probing small differences in the geometry of coordination (i.e., variation on bonding angle or movement of axial ligand around the Cu center). Their presence confirms the anisotropic character of the symmetry.

Information provided by the simulations

Because it is difficult to rationalize the XANES features of these spectra with a qualitative analysis only, we have started simulations of the absorption coefficient in the XANES region, in the MS approach, with the G4XANES package (Durham et al., 1982) and the CONTINUUM code (Tyson et al., 1992). In accordance with the previous MS calculations of cobalt-substituted-Hc and oxy-Hc (Della Longa et al., 1993), we are considering scattering clusters that include the three imidazole rings around the copper site (E. Borghi, unpublished).

The size of the scattering cluster is a key factor of XANES simulations. In effect, by considering progressively increasing cluster sizes starting from the first-shell atoms, the calculations show that, although the A, B, C peaks arise from the first shell, the D peak reflects the whole geometry of the copper site. So, a red shift of the position of main peak D can reflect a major isotropic character of the structure and a different geometry of coordination. A low-intensity ratio between the peaks C and D (i.e., δ feature more intense) can reflect a lowering of the coordination number in the cluster. A different ratio between the β and γ peaks should involve changes in the first-shell coordination geometry (Bianconi, 1988).

The simulations on oxy-Hc (Della Longa et al., 1993) have been able to clarify and to assign the polarization dependence of the XANES features: peaks A and B are assigned to a final state $4p_z$, whereas peaks C and D to the $4p_{xy}$ state. Furthermore, MS calculations starting from the oxy- and deoxy-forms of Hcs have been able to reproduce the XANES spectra of alternative five-coordinated structures of this copper(II) site (Della Longa et al., 1993, 1996). In particular, they enabled correlation of the red shift of the β peak, and the associated variation of the relative-intensity ratio of the α and γ peaks, to a longer bond distance of the apical ligand, i.e., from 11.5 eV (d = 1.9 Å) to 1.5 eV (d = 2.7 Å), and thus to an apical distortion of the standard structure of oxy-form (square-pyramidal copper site geometry). So, the resulting d (Å) versus $E - E_0$ (eV) correlation can provide a qualitative criterion to understand the structural characteristics of the Hcs derivatives and of the related model compounds considered in our study.

Comparative analysis of model compounds and Hcs derivatives

In the case of the two monomeric models of the 2-BB ligand, the features of the XANES spectra (Fig. 9) are in agreement with the x-ray data. The peak P indicates the noncentro-symmetric character of the two metal centers. The shape and the energy position of the features of the same type differ for the two compound, indicating different coordination geometry: the spectrum of 2-BB azide compound presents clearly the A, B, C, D features and a major intensity of the δ peak. This reflects the four-coordination in the 2-BB-N_3 case with respect to the five-coordination for the 2-BB-$(H_2O)_2$ compound and the difference of their symmetries.

All the XANES spectra of the binuclear model compounds are complicated and show differences between the homologous of the two ligands L-5,5 and L-6,6 (Figs. 7 and 8). A qualitative discussion is possible only inside the same ligand family. The absorption shapes for all the L-5,5 complexes are compatible with five-coordinated Cu clusters in accordance with the x-ray results (L. Casella, Univ. Pavia, Italy, personal communication) for the L-55 bis(hydroxo) complex. So all the L-5,5 complexes are showing a similar geometry. In the case of the L-5,5-$(OH)_2$, the form of the derivative and the position of the β peak suggest the presence of an axial distortion inside a noncentro-symmetric Cu cluster (P feature). An apical distance of ~2.5 Å is estimated in agreement with the x-ray data of the metoxy analog. The shapes of L-5,5-$(H_2O)_2$ and L-5,5-N_3 appear different in the edge and in the main peak region (the C feature is more clearly present). This indicates a different axial symmetry in these Cu site(s) with respect to that of bis-hydroxo (see Fig. 7). Shorter apical distances can be estimated from the position of the β peaks, i.e., ~2.3 Å for L-5,5-$(H_2O)_2$ and ~2.4 Å for L-5,5-N_3.

The absorption shapes of the L-6,6 compounds, by comparison to the homologous derivative of L-5,5 ligand, are compatible with an overall five-coordination number at the Cu site(s) and similar noncentro-symmetric character (P feature). The L-6,6 ligand presents a higher flexibility with respect to the L-5,5, so, in this family, the structure of the Cu clusters are expected to reveal a more isotropic character with respect to that of L-5,5. The ϵ and φ derivative features, clearly evident as in the L-5,5 family, are an indicator of the anisotropic character of the symmetry of these complexes. However, in the L-6,6 family, the shape and intensity of the ϵ feature differ, indicating some differences inside the conformational details of the geometry of coordination. In the L-6,6 family (see Fig. 8) the major differences are in the region of the main peaks, C and D, suggesting diversities in the axial geometry at the Cu sites with respect to the L-5,5 analog. The form of the derivatives and the position of the β peaks propose the presence of a minor distortion for which a value of ~2.3 Å can be estimated similar within the L-6,6 family. The more intense δ features suggest a smaller number of Z-donor in the first shell for L-6,6-N_3 and L-6,6-$(H_2O)_2$ with respect to the L-6,6-$(OH)_2$.

By comparing the XANES features for the Hcs (Fig. 6) we see significant differences between homologous derivatives. Evident changes are present in the XANES spectra of the met-azido-Hcs with respect to the corresponding met-Hcs forms. There are differences also with respect to the model compounds (see Figs. 7 and 8). This implies differences on chromophores of the met-forms and of the azide adducts of the proteins with respect to the homologous models. The absorption shape of all Hc derivatives indicates an overall five-coordination number at the Cu site(s) with noncentro-symmetric character (P feature). In any case, the met-Hcs spectra resemble those of the L-6,6-$(OH)_2$ and L-6,6-$(H_2O)_2$ models, suggesting a similar anisotropic character of the overall symmetry (see shape and position of the ϵ and φ derivative features), but different local conformation (see shape and position of the α, β, γ, δ peaks) with respect to the structure of these complexes. The similarities seem to be major with the bis(hydroxo) complex. From the position of the β peaks, the presence of an apical ligand distance between 2.3 and 2.4 Å can be proposed for the met- and met-azido-Hc forms. The met-azido-Hcs spectra are different from those of both L-N_3 and 2-BB-N_3. However, the shapes of the derivatives indicate a greater similarity between the met-N_3 from *O. vulgaris* and the L-6,6-N_3 model (μ-1,3 bridging mode).

The case of the *C. aestuarii* derivative is more complex. There is some correspondence of shape and position at high energy (ϵ and φ derivative features) and at low energy (α and β features in the L-6,6 case only) with the azide models of the 2-BB and L-6,6 ligands. Both ligands provide 6-T chelate rings and similarities of the met-Hc derivative of both phyla with the L-6,6 family have been observed. However, with respect to the 2-BB-N_3 model (end-on binding mode), the coordination number for the *Carcinus* met-azido-Hc derivative is expected to be five, and the symmetry of the Cu cluster should be different. These differences appear clearly when comparing the shape and the position of the other peaks. The similarities with the L-6,6-N_3 model (μ-1,3 bridging mode) propose analogous constraints and the presence of a μ-bridge for the binding of azide, but the differences noted suggest a different coordination fashion of the bridge. By comparing the XANES features of the L-5,5-N_3 model (μ-1,1 bridging mode, 5-T chelate rings) and the met-N_3 derivative from *C. aestuarii*, we see differences, which could be attributed to the different constrains imposed by the L-5,5 ligand and by the protein matrix. The mode of coordination proposed by the L-5,5 model complex cannot be excluded. The spectroscopic model (Alzuet et al., 1997) suggested an end-on geometry, and, in this case, two different symmetries can be present at the copper site. The

results obtained for the met-azido-Hc derivative of *C. aestuarii* require a very careful MS XANES calculation because the XANES spectrum is expected to contain information on each copper site.

CONCLUDING REMARKS

The EXAFS analysis of the first shell, in combination with a qualitative XANES analysis and the preliminary results of the MS analysis, is allowing us to establish some conclusions on our general study of the oxidized-Hc derivatives and on their related models. The results obtained for the mononuclear compounds and for the binuclear L-5,5-bis(hydroxo) complex, which are in agreement with the data of the crystallographic structures, validate the approach followed for the analysis of data. The results obtained for the remaining poly(benzimidazole)-complexes (with unknown structure) are compatible with previous spectroscopic studies (Casella et al., 1993). The L-6,6-bis(hydroxo) complex is characterized by a shorter apical distance, but the binuclear copper(II) centers with the two ligands present similar bis(hydroxo)-bridged structure. The results obtained on the aquo complexes seem to confirm the presence of a bis(aquo)-bridge structure as suggested by previous NMR studies. The XANES features are suggesting an overall symmetry of the Cu clusters similar to the correspondent bis(hydroxo) centers, but with some local differences. This is in agreement with the EXAFS results for which one of the two water molecules is at a longer distance with respect to the hydroxo complexes, thus bridging the $Cu_2(H_2O)_2$ units to a less rigid conformation. The hints that we have from the first analyses for the azide compounds suggest a similarity with the aquo compounds. The values of the L-5,5-azido are in agreement with a μ-1,1 coordination and the presence of a second bridge. The L-6,6-N_3, clearly, shows a coordination mode of the anion different with respect to the L-5,5 case. The results obtained seem to be compatible with a μ-1,3 binding mode for the azide and with the presence of a second bridge.

In the case of the proteins, the work presented here extends our knowledge of the met-Hc compounds by favoring the hypothesis of a bis(hydroxo) structure for both species and thus discerning the origin of the magnetic coupling of the site. The EXAFS results that are similar, at this pH, for the *O. vulgaris* and *C. aestuarii* Hc met forms do not explain the catalase activity present in the met forms of molluscs with the coordination number, type of ligands, and bond distances. The results obtained for the met-azido-Hcs are in agreement with previous spectroscopic characterizations (*Octopus* derivative), but are still ambiguous and require a very careful MS calculation for the *C. aestuarii* derivative. By comparing the XAS features of the met-azido-Hcs derivatives to those of the model compounds, it seems possible to confirm the μ-bridging mode for *O. vulgaris* previously proposed (Beltramini et al., 1995). The μ-1,3 appears more probable. The XAS features for a terminal binding mode and for a μ-1,1 bridging mode present some structural similarity. Therefore, the result of *C. aestuarii* derivative, for which the reaction models for the binding of azide propose a terminal mode (Alzuet et al., 1997), is not yet fully clarified.

This investigation allowed the determination of a correct value of the Cu–Cu distance. The features of the XANES edge region and the EXAFS analysis in the MS approach validate an apical distortion at the copper site, as a consequence of the movement of the apical ligand involved in the ligand association.

The authors are grateful to Prof. L. Casella (University of Pavia, Italy) for the kind gift of all model compounds and for the private communication on x-ray data of one model compound.

This work was supported by the grant 9803184222 from the Ministero dell'Università e della Ricerca Scientifica, Italy (to E.B. and P.L.S.) and by a French Government fellowship to P.L.S. Our research project was partially supported, under the decision of the European Committee, by the European Synchrotron Radiation Facility in Grenoble, France.

REFERENCES

Alzuet, G., L. Bubacco, L. Casella, G. P. Rocco, B. Salvato, and M. Beltramini. 1997. The binding of azide to copper-containing and cobalt-containing forms of hemocyanin from the Mediterranean crab *Carcinus aestuarii. Eur. J. Biochem.* 247:688–694.

Ascone, I., A. Sabatucci, L. Bubacco, P. Di Muro, and B. Salvato. 2000. Saccharose solid matrix embedded proteins: a new method for sample preparation for x-ray absorption spectroscopy. *Eur. Biophys. J.* 29: 391–397.

Beltramini, M., L. Bubacco, B. Salvato, L. Casella, M. Gullotti, and S. Garofani. 1992. The circular dichroism spectrum as a probe for conformational changes in the active site environment of hemocyanins. *Biochim. Biophys. Acta.* 1120:24–32.

Beltramini, M., L. Bubacco, L. Casella, G. Alzuet, M. Gullotti, and B. Salvato. 1995. The oxidation of hemocyanin. Kinetics, reaction mechanism and characterization of Met-hemocyanin product. *Eur. J. Biochem.* 232:98–105.

Bianconi, A. 1988. XANES spectroscopy. *In* X-Ray Absorption Principles, Applications, Techniques of EXAFS, SEXAFS and XANES. D. C. Koningsberger, and R. Prinz, editors. J. Wiley and Sons, New York. 573–662.

Bubacco, L., R. S. Magliozzo, M. Beltramini, B. Salvato, and J. Peisach. 1992. Preparation and spectroscopic characterization of a coupled binuclear center in cobalt(II)-substituted hemocyanin. *Biochemistry.* 34: 9294–9303.

Casella, L., O. Carugo, M. Gullotti, S. Garofani, and P. Zanello. 1993. Hemocyanin and tyrosinase models. Synthesis, azide binding and electrochemistry of dinuclear copper(II) complexes with poly(benzimidazole) ligands modelling the Met forms of the proteins. *Inorg. Chem.* 32:2056–2067.

Casella, L., O. Carugo, M. Gullotti, S. Doldi, and M. Frassoni. 1996. Synthesis, structure, and reactivity of model complexes of copper nitrite reductase. *Inorg. Chem.* 35:1101–1113.

Cuff, M. E., K. I. Miller, K. E. van Holde, and W. A. Hendrickson. 1998. Crystal structure of a functional unit from *Octopus* hemocyanin. *J. Mol. Biol.* 278:855–870.

Della Longa, S., A. Bianconi, L. Palladino, B. Simonelli, A. Congiu Castellano, E. Borghi, M. Barteri, M. Beltramini, G. P. Rocco, B. Salvato, L. Bubacco, R. S. Magliozzo, and J. Peisach. 1993. An X-ray absorption near edge structure spectroscopy study of metal coordination

in Co(II)-substituted *Carcinus maenas* hemocyanin. *Biophys. J.* 65: 2680–2691.

Della Longa, S., I. Ascone, A. Bianconi, A. Bonfigli, A. Congiu Castellano, O. Zaviri, and M. Miranda. 1996. The dinuclear copper site structure of *Agaricus bisporus* tyrosinase in solution probed by x-ray absorption spectroscopy. *J. Biol. Chem.* 271:21025–21030.

Durham, P. J., J. B. Pendry, and C. H. Hodges. 1982. Calculation of x-ray absorption near-edge structure, XANES. *Comput. Phys. Commun.* 25: 193–205.

Eicken, C., F. Zippel, K. Büldt-Karentzopoulos, and B. Krebs. 1998. Biochemical and spectroscopic characterization of catechol oxidase from sweet potatoes (*Ipomoea batatas*) containing a type-3 dicopper center. *FEBS Lett.* 436:293–299.

Feiters, M. C. 1990. X-ray absorption spectroscopic studies of metal-coordination in zinc and copper proteins. *Comments Inorg. Chem.* 11: 131–174.

Feiters, M. C., R. J. M. Klein Gebbink, V. A. Solé, H. F. Nolting, K. D. Karlin, and R. J. M. Nolte. 1999. X-ray absorption spectroscopic studies of the copper(I) complexes of crown ether appended bis{(2-pyridyl)ethyl}amines and their dioxygen adducts. *Inorg. Chem.* 38: 6171–6180.

Felsenfeld, G., and M. P. Prinz. 1959. Specific reaction of hydrogen peroxide with the active site hemocyanin. The formation of Met-hemocyanin. *J. Am. Chem. Soc.* 81:6259–6264.

Filipponi, A., A. Di Cicco, and C. R. Natoli. 1995. X-ray absorption spectroscopy and n-body distribution functions in condensed matter. I: Theory. *Phys. Rev. B.* 52:15122–15134.

Filipponi, A., and A. Di Cicco. 1995. X-ray absorption spectroscopy and n-body distribution functions in condensed matter. II: Data analysis and applications. *Phys. Rev. B.* 52:15135–15149.

Fonda, E., A. Michalowicz, L. Randaccio, G. Tauzher, and G. Vlaic. 2001. EXAFS data analysis of vitamin B12 model compounds: a methodological study. *Eur. J. Inorg. Chem.* 2001:1269–1278.

Hasnain, S. S., and K. O. Hodgson. 1999. Structure of metal centres in proteins at subatomic resolution. *J. Synchrotron Rad.* 6:852–864.

Hazes, B., K. A. Magnus, C. Bonaventura, J. Bonaventura, Z. Dauter, K. H. Kalk, and W. G. Hol. 1993. Crystal structure of deoxygenated *Limulus polyphemus* subunit II hemocyanin at 2.18 angstroms resolution: clues for a mechanism for allosteric regulation. *Protein Sci.* 2:597–619.

Himmelwright, R. S., N. C. Eickman, C. D. Lubien, and E. I. Solomon. 1980. Chemical and spectroscopic comparison of the binuclear copper active site of mollusc and arthropod hemocyanin. *J. Am. Chem. Soc.* 102:5376–5388.

Kahn, O., S. Sikorav, J. Gouteron, S. Jeannin, and Y. Jeannin. 1983. Crystal structure and magnetic properties of (μ-azido)(μ-hydroxo)-bis[(*N*,*N*,*N*′,*N*′-tetramethylethylenediamine)copper(II)]perchlorate, acopper(II) dinuclear complex with a large ferromagnetic interaction. *Inorg. Chem.* 22:2877–2883.

Kau, L. S., D. J. Spira-Solomon, J. E. Penner-Hahn, K. O. Hodgson, and E. I. Solomon. 1987. X-ray absorption edge determination of the oxidation state and coordination number of copper: application to the type 3 site in *Rhus vernicifera* laccase and its reaction with oxygen. *J. Amer. Chem. Soc.* 109:6433–6442.

Kitajima, N., K. Fujisawa, S. Hikichi, and Y. Moro-oka. 1993. Formation of (μ-hydroxo)(μ-azido) dinuclear copper complex from μ-η^2:η^2-peroxo complex. *J. Am. Chem. Soc.* 115:7874–7875.

Lee, P. A., and J. B. Pendry. 1975. Theory of the extended x-ray absorption fine structure. *Phys Rev. B.* 11:2795–2811.

Lengeler, B., and P. Eisenberger. 1980. Extended x-ray absorption fine structure analysis of interatomic distances, coordination numbers and mean relative displacements in disordered alloys. *Phys. Rev. B.* 21: 4507–4520.

Ling, J., L. P. Nestor, R. S. Czernuszewicz, T. C. Spiro, R. Fraczkiewicz, K. D. Sharma, T. M. Loehr, and J. Sanders-Loehr. 1994. Common oxygen binding site in hemocyanins from arthropods and molluscs. Evidence from Raman spectroscopy and normal coordinate analysis. *J. Am. Chem. Soc.* 116:7682–7691.

Lynch, W. E., D. M. Kurtz, Jr., S. Wang, and R. A. Scott. 1994. Structural and functional models for the dicopper site in hemocyanin. Dioxygen binding by copper complexes of Tris(1-R-4-R′-imidazolyl-kN)phosphines. *J. Am. Chem. Soc.* 116:11030–11038.

Mc Kale, A. G., B. W. Veal, A. P. Paulikas, S. K. Chan, and G. S. Knapp. 1988. Improved ab initio calculations of amplitude and phase functions for extended x-ray absorption fine structure spectroscopy. *J. Am. Chem. Soc.* 110:3763–3768.

Meneghini, C., and S. Morante. 1998. The active site structure of tetanus neurotoxin resolved by multiple scattering analysis in x-ray absorption spectroscopy. *Biophys. J.* 75:1953–1963.

Michalowicz, A. 1990. Methodes et programmes d'analyse des spectres d'absorption des rayons X (EXAFS). Applications à l'étude de l'orde local et du desordre cristallin dans les materiaux inorganiques. Ph.D. thesis. Paris–Val de Marne University, Paris.

Palladino, L., S. Della Longa, A. Reale, M. Belli, A. Scafati, G. Onori, and A. Santucci. 1993. XANES of Cu(II)-ATP and related compounds in solution: quantitative determination of the distortion of the Cu site. *J. Chem. Phys.* 98:2720–2726.

Pascarelli, S., F. Boscherini, F. D'Acapito, J. Hardy, C. Meneghini, and S. Mobilio. 1996. X-ray optics of a dynamical sagittal-focusing monochromator on the GILDA beam-line at the ESRF. *J. Synchrotron Rad.* 3:147–155.

Pickering, I. J., and G. N. George. 1995. Polarized x-ray absorption spectroscopy of cupric chloride dihydrate. *Inorg. Chem.* 34:3142–3152.

Sabatucci, A., I. Ascone, L. Bubacco, M. Beltramini, P. Di Muro, and B. Salvato. 2002. Comparison of the x-ray absorption properties of the binuclear active site of molluscan and arthropodan hemocyanins. *J. Biol. Inorg. Chem.* 7:120–128.

Salvato, B., and M. Beltramini. 1990. Hemocyanins: molecular architecture, structure and reactivity of the binuclear copper active site. *Life Chem. Rep.* 8:1–47.

Sano, M., S. Komorita, and H. Yamatera. 1992. XANES spectra of copper(II) complexes: correlation of the intensity of the 1s→3d transition and the shape of the complex. *Inorg. Chem.* 31:459–463.

Scott, R. A., and M. K. Eidsness. 1988. The use of x-ray absorption spectroscopy for detection of metal–metal interactions. Application to copper-containing enzymes. *Comments Inorg. Chem.* 7:235–267.

Shadle, S. E., J. E. Penner-Hahn, H. J. Schugar, B. Hedman, K. O. Hodgson, and E. I. Solomon. 1993. X-ray absorption spectroscopic studies of the blue copper site: metal and ligand K-edge studies to probe the origin of the EPR hyperfine splitting in plastocyanin. *J. Am. Chem. Soc.* 115:767–776.

Solomon, E. I., M. J. Baldwin, and M. D. Lowery. 1992. Electronic structures of active sites in copper proteins: contributions to reactivity. *Chem. Rev.* 92:521–542.

Solomon, E. I., and M. D. Lowery. 1993. Electronic structure contribution to function in bioinorganic chemistry. *Science.* 259:1575–1581.

Tyson, T. A., K. O. Hodgson, C. R. Natoli, and M. Benfatto. 1992. General multiple-scattering scheme for the computation and interpretation of X-ray absorption fine structure in atomic clusters with applications to SF_6, $GeCl_4$, and Br_2 molecules. *Phys. Rev. B.* 46:5997–6019.

van Holde, K. E., and K. I. Miller. 1995. Hemocyanins. *In* Advances in Protein Chemistry. Academic Press Inc., Orlando, FL. 1–81.

Volbeda, A., and W. G. J. Hol. 1989. Crystal structure of hexameric haemocyanin from *Panulirus interruptus* refined at 3.2 Angstroms resolution. *J. Mol. Biol.* 209:249–279.

Woolery, G. L., L. Powers, M. Winkler, E. I. Solomon, and T. G. Spiro. 1984. EXAFS studies of binuclear copper site of oxy-, deoxy-, metaquo-, metfluoro-, and metazido-hemocyanin from arthropods and molluscs. *J. Am. Chem. Soc.* 106:86–92.

Zlateva, T., L. Santagostini, L. Bubacco, L. Casella, B. Salvato, and M. Beltramini. 1998. Isolation of the Met-derivative intermediate in the catalase-like activity of deoxygenated *Octopus vulgaris* hemocyanin. *J. Inorg. Biochem.* 72:211–219.